Nanoscale Advances

ROYAL SOCIETY OF CHEMISTRY

PAPER

View Article Online
View Journal | View Issue

Cite this: *Nanoscale Adv.*, 2023, **5**, 7077

Hybrid AuNPs-3MPS-MTX nanosystem and its evaluation for treating cervical cancer and melanoma

M. J. Hernández-Esparza,[ab] Ilaria Fratoddi,[b] Sara Cerra,[b] K. Juarez-Moreno *[c] and R. Huirache-Acuña *[a]

Received 6th August 2023
Accepted 16th November 2023

DOI: 10.1039/d3na00605k

rsc.li/nanoscale-advances

This research presents an evaluation of a hybrid material based on gold nanoparticles (AuNPs), stabilized with the thiol 3-mercapto-propanesulfonate (3MPS) and loaded with the methotrexate drug (MTX). The AuNPs-3MPS-MTX nanosystem was tested for the treatment of cervical cancer and melanoma, using the B16-F10 melanoma and HeLa cell lines. The tests performed on cell cultures assessed the efficiency of the studied nanosystem on tumor cells, as well as its toxicology.

1. Introduction

Currently, the use of nanotechnology in the biomedical field has generated significant interest in diagnosing and treating certain important diseases, such as cancer. This interest arises due to the reported toxic effects of drugs for cancer treatment. In this context, the selection of an appropriate transport system for releasing the active substance plays a crucial role. Nanotechnology not only improves the solubility, stability, and biodistribution[1] of the drug but also allows for minimally invasive drug release. The ability to manufacture nanoscale devices facilitates their passage through pores and cell membranes. Moreover, controlling the drug release enhances its effectiveness, making it essential to consider the required dose, size, morphology and surface properties of the compound. When nanoparticles are able to associate with specific organs, tissues, or damaged cells and release the active ingredient *in situ*, the drug's toxicity can be reduced. On the other hand, the gradual release of the drug based on the patient's needs helps mitigate possible adverse events that may arise from uncontrolled direct drug delivery.[2,3]

The use of nanoparticulate drugs enables achieving levels of supersaturation that were previously attainable only when switching from a crystalline to an amorphous drug. Particle size plays a crucial role in the dissolution rate of drugs. Reducing the particle size can significantly increase the dissolution rate and, consequently, enhance bioavailability.[4] This effect may lead to a better bioavailability of the drug. If the nanoparticle is coated with a polymer, the release is controlled by the diffusion of the drug through the polymeric membrane, making the membrane coating act as a release barrier.

Gold nanoparticles (AuNPs) have demonstrated their utility as both drug delivery carriers and diagnosis platforms due to their size, lack of toxicity, easy functionalization, and high surface area to volume ratio.[5] The usage of AuNPs has enhanced the effectiveness of anticancer therapies by augmenting the drug delivery to the tumor, owing to their distinctive physicochemical properties. Other studies have highlighted the potential of AuNPs, either as biocompatible drug carriers or as enhancers to boost therapeutic effectiveness. For instance, platinum-linked AuNPs exhibited cytotoxicity in A549 lung cancer cell line.[5] Furthermore, a doxorubicin-AuNPs complex induced apoptosis and upregulated tumor-suppressing genes in A549 cells.[6] Moreover, AuNPs loaded with paclitaxel have shown their effectiveness compared to free drug to induce cytotoxicity in MCF-7 and MDA-MB-231 breast cancer cells and the noncancerous HEK293 cell line. These AuNPs demonstrated lower toxicity in normal cells than breast cancer cells.[7] Retinoic acid-PEG-thiol-conjugated AuNPs exhibited sixfold greater potency than retinoic acid polyethylene glycol-thiol alone when administered at the same dose on cervical cancer cells.[8] Additionally, Paino *et al.*, conducted a comparative analysis of the cytotoxic effects of AuNPs coated with either sodium citrate or polyamidoamine (PAMAM) dendrimers on HepG2 hepatoma cells and normal peripheral blood mononuclear cells (PBMCs).[9] The utilization of 15 nm AuNPs carrying cisplatin led to a significant reduction in the density of colorectal-cancer-associate fibroblasts (CAFs).[10] In summary, the stability and biocompatibility demonstrated by the AuNPs complex imply that it could hold great promise as a therapeutic approach for addressing different types of cancer.

Developing a nanoformulation based on ultrafine AuNPs conjugated with MTX, led to improved drug effectiveness and

[a]*Facultad de Ingeniería Química, Universidad Michoacana de San Nicolás de Hidalgo, Ciudad Universitaria, C.P. 58060, Morelia, Mexico. E-mail: rafael.huirache@umich.mx*

[b]*Department of Chemistry, University Sapienza of Rome, p. Aldo Moro 5, 00185 Rome, Italy*

[c]*Centro de Física Aplicada y Tecnología Avanzada, Universidad Nacional Autónoma de México, Mexico. E-mail: kjuarez@fata.unam.mx*

minimal toxicity in breast cancer treatment. The ultra-small size of AuNPs (5 nm) facilitated enhanced uptake.[11] Compared to other nanoplatforms, the AuNPs-3MPS-MTX hybrid system exploits its ability in cancer treatment due to the presence of loaded MTX (an anticancer drug), whereas other nanomaterial-based cancer therapies such as ferroptosis-related oxidation effect,[12] oxidative stress amplification,[13] and heat-induced light irradiation (photothermal and photodynamic therapies)[14] do not rely on the presence of a specific drug on the nanostructures, thus being less specific. The high surface-to-volume ratio opens to multiple functionalization both *in situ* and *ex situ* with different bioactive and targeting agents.[15] Furthermore, nanostructured gold is not prone to oxidation compared to other free metal ions (*e.g.*, Fe^{2+}, Cu^{2+} *etc.*) and showed[16] significant penetration ability in cancerous cells up to 70%. Additionally, the ability to control their size and functionalization has been studied by Bessar *et al.* who examined the efficiency of MTX-AuNPs for treating psoriasis.[17] As physicochemical attributes play an important role in the diffusion of NPs, there is a concern about finding synthesis methodologies that influence these attributes and are efficient for subsequent applications. Therefore, this research project focuses on studying the formulation and evaluation of a hybrid material based on gold nanoparticles (AuNPs), stabilized with the hydrophilic thiol 3-mercapto-propanesulfonate (3MPS) and loaded with the methotrexate drug (MTX). As reported, short and negatively charged functionalizing agents showed better intracellular uptake levels on human skin keratinocyte (HaCaT) keratinocytes and human epithelial colorectal adenocarcinoma (Caco-2) cells, compared with long PEG-COOH and PEG-NH_2 capped AuNPs.[18] Thus, the 3MPS thiol was chosen as stabilizing/functionalizing agent of AuNPs since it shows several advantages compared to other surface ligands: (i) the –SH ending group ensures a covalent functionalization *via* Au-S bond preventing the release of the surface agent during applicative studies, (ii) bearing a negatively charged $-SO_3^-$ group it confer an hydrophilic behavior to final AuNPs colloid, essential in biomedical applications, and (iii) the sulfonate moiety has been identified as the primary counterpart for MTX interaction *via* electrostatic forces.[19] Moreover, AuNPs-3MPS and AuNPs-3MPS-MTX tested *in vitro* on skin model and *in vivo* studies on imiquimod-induced psoriasis-like mice, did not show cytotoxicity inducing a decrease in the severity of erythema and scaling of skin lesions in treated mice.[17,20] The as-synthesized AuNPs with size approx. 5 nm, contain approximatively 720 thiol molecules on a single nanoparticle and the drug loaded sample, AuNPs-3MPS-MTX showed a loading percentage of 80 ± 5%, with a release of 80% in an hour and up to 95% in 24 hours.[17] To the best of our knowledge, there are no references in the literature regarding the use of this AuNPs-3MPS-MTX nanosystem for the treatment of cervical cancer and melanoma.

2. Experimental

The AuNPs-3MPS-MTX hybrid nanosystem used in this project was synthesized and characterized previously[19] by S. Cerra, *et al.* (2020), and surface morphology before and after MTX interaction was verified with field-emission scanning electron microscopy (FESEM) AURIGA Zeiss, sampling suspensions by drop-casting on Al stub. In this work, the biomedical *in vitro* application for the treatment of cervical cancer and melanoma was studied.

Cell culture

Mouse melanoma cell line B16-F10 (ATCC CRL-6475) and HeLa cells are cultured in DMEM (Dulbecco's Modified Eagle's Medium) supplemented with 10% v/v fetal bovine serum (FBS), 1% v/v streptomycin/penicillin, 1% v/v L-glutamine and sodium bicarbonate (2 g L^{-1}), adjusted to a pH of 7.4, and sterilized by filtration through a filter with a pore size of 0.22 μm. Cells were maintained in Petri dishes for cell culture at 37 °C in an atmosphere of 5% CO_2 until confluency.

Cell viability tests by MTT reduction

The cell viability assay by MTT reduction was performed on a 96-well plate, in which 10 000 cells were seeded in each well, in a final volume of 100 μL of DMEM, and then incubated for 24 hours at 37 °C in an atmosphere of 5% CO_2. Subsequently, the culture medium was discarded and different concentrations of AuNPs-3MPS, AuNPs-3MPS-MTX and MTX (0, 1, 2, 4, 8, 16, 32, and 64 μg mL^{-1}) were added to each well in triplicate in a final volume of 100 μL of cell culture medium, and then incubated for 48 hours at 37 °C in an atmosphere of 5% CO_2. Cells cultivated with cell media was used as positive control, while cells exposed to TritonX-100 at 0.5% (v/v) were used as negative controls. Afterward, the culture medium was decanted from the plate and the cells were washed three times with 200 μL of phosphate buffer (PBS 1x), then 10 μL of MTT (5 mg mL^{-1}) and 90 μL of culture medium were added to each well, the plate was incubated for 4 hours at 37 °C in an atmosphere of 5% CO_2. After this, 100 μL of pure isopropanol was added to each well, and the sample was re-suspended several times with the aid to dissolve the formazan crystals, then the plate was incubated for 30 minutes at room temperature and in the dark. Finally, the absorbance of formazan was measured at a wavelength of 570 and 690 nm on a Thermo Scientific Multiskan GO ELISA plate reader. To calculate the cell viability, the absorbance of samples at 690 nm was subtracted from the absorbance at 570 nm. The absorbance value of the positive control was taken as 100% of cell viability; from there, the corresponding percentage was calculated for each well.

Detection of reactive oxygen species (ROS)

Through the evaluation of the production of reactive oxygen species (ROS) it is possible to determine whether nanoparticles are capable of inducing significant oxidative stress in cell lines exposed to different concentrations of the AuNPs-3MPS, and AuNPs-3MPS-MTX and MTX free-drug. Therefore, using the Image-IT Live Green Reactive Oxygen Species Detection Kit (I36007, Invitrogen), it was possible to measure by flow cytometry the fluorescence of CFDA, a reagent that is reduced by the ROS generated in the cytoplasm of the cell.

Cell culture for the detection of ROS

For this assay, each cell line was seeded in a 12-well plate at a density of 150 000 cells per well and incubated for 48 h at 37 °C in an atmosphere of 5% CO_2 with different concentrations of AuNPs-3MPS, AuNPs-3MPS-MTX and MTX (0, 1, 2, 4, 8, 16, 32, and 64 μg mL^{-1}). After this, cells were harvested, and the cell pellet was resuspended in 250 μL of DMEM with the reagent carboxyH_2-DCFDA (25 μM) and incubated at 37 °C in an atmosphere of 5% CO_2 for 1 hour. To measure the intrinsic production of ROS, cells were solely cultivated in DMEM, while to induce oxidative stress; cells were exposed to 50 μM of *tert*-butyl hydroperoxide (TBHP) for 24 hours. After incubation, cells were centrifuged at 1200 rpm for 5 minutes, the supernatant was removed, and the pellet was resuspended in 1 mL of PBS. Finally, the cells were analyzed by flow cytometry with an Attune NxT cytometer using the BL1 fluorescence channel (Excitation 488 nm/Emission 525 nm). The data recorded were of at least 30 000 events for each sample with their respective triplicates. Data were analyzed using the Attune NxT software version 3.2.1 (Life Technologies, Thermo Fisher Scientific, Waltham, MA, USA).

Cell membrane permeability

After exposing the cells to various concentrations of MTX, AuNPs-3MPS and AuNPs-3MPS-MTX, the cells were collected and suspended in 200 μL of PBS. Subsequently, the cells were incubated at 25 °C for 30 min with propidium iodide (PI) to assess cell membrane permeability. Following this incubation, the cells were rinsed thrice with PBS and subjected to further analysis using flow cytometry. The data were acquired from the examination of at least 10 000 events, with PI detection performed at BL3 channel using the Attune NxT flow cytometer (Life Technologies, Carlsbad, CA, USA) and analyzed using the Attune NxT acquisition software version 3.2.1 (ThermoFisher).

Apoptosis and necrosis cell death assay

Cell death, either through apoptosis or necrosis induced by the incubation of HeLa and B16-F10 cells with different concentrations of MTX, AuNPs-3MPS and AuNPs-3MPS-MTX, was measured by flow cytometry with fluorescein isothiocyanate (FITC)-annexin V and propidium iodide (PI) staining, using the Annexin V-FITC apoptosis detection kit (Thermo Fisher Scientific, Waltham, MA, USA).

AuNPs uptake assessments

To assess the cellular uptake of AuNPs-3MPS, AuNPs-3MPS-MTX and MTX, we conducted a comparison of cell granularity using flow cytometry. The internalization of nanoparticles was evaluated by comparing the side scatter values of cell samples, as previously documented.[21] We seeded a density of 4×10^5 cells in a 12-well plate and cultured them for 24 hours at 37 °C with 5% CO_2. Subsequently, the cells were washed with PBS and incubated with AuNPs-3MPS, AuNPs-3MPS-MTX and MTX at a concentration of 1 to 64 μg m^{-1} for 48 hours under the same conditions. Afterward, the cells underwent three PBS washes, were harvested using Trypsin/EDTA (Sigma Aldrich, MO, USA), and resuspended in 1 mL of PBS. The samples were then analyzed using flow cytometry with an Attune NxT flow cytometer (Life Technologies, Carlsbad, CA). Flow cytometry data were collected from at least 10 000 events (cells) and analyzed based on forward scatter (FSC) and side scatter (SSC) signals using the Attune NxT software (Life Technologies).

Statistical analysis

All the experiments were performed in threefold independent manner with internal triplicates. The data were statistically analyzed using GraphPad Prism software version 10.0 (San Diego, CA, USA) through an analysis of variance ANOVA, followed by Tukey's multiple comparison test. The results were plotted as the mean ± standard deviation of three independent experiments and were considered statistically significant when $p < 0.05$.

3. Results and discussion

Cell viability of HeLa cells and B16-F10 melanoma cells

The percentage of cell viability for B16-F10 and HeLa cancer cells in the presence of AuNPs (AuNPs-3MPS), AuNPs-3MPS-MTX and MTX at different concentrations (1, 2, 4, 8, 16, 32, 64 μg mL^{-1}) is presented in Fig. 1. It can be observed that the exposure of both cell lines to all concentrations of AuNPs does not induce significant cytotoxicity. However, the AuNPs-3MPS-MTX hybrid nanosystem caused a significant decrease in cell viability in both cell lines in a concentration-dependent manner. Indeed, at higher system concentrations, cell viability diminished by almost 70% for both B16-F10 and HeLa cells. Additionally, it was observed that the drug methotrexate (MTX) induced less cytotoxicity than the bioconjugate AuNPs-3MPS-MTX, indicating that nanosystem do not affect the vectorization of the drug.

Cell membrane permeability of B16-F10 and HeLa cells

Fig. 2 depicts the percentage of permeabilized cells for both cell lines concerning the concentrations used for each treatment. Using AuNPs with the active substance resulted in significantly higher cell permeabilization at a concentration of 32 μg mL^{-1} compared to its counterpart without MTX and MTX drug alone. As previously mentioned[19] by S. Cerra, *et al.* (2020), the synthesis of AuNPs-3MPS-MTX provides a nanosystem that improves the penetration of the MTX drug inside cells during cells' permeability studies. On the other hand, when studying HeLa cells, it was observed that MTX induces a higher cells' permeabilization then the effect elicited by AuNPs-3MPS-MTX.

ROS generation from HeLa cells and B16-F10 melanoma cells

Fig. 3 illustrates the intracellular percentage of ROS produced in HeLa cells and B16-F10 melanoma cells when incubated with AuNPs (AuNPs-3MPS), AuNPs-3MPS-MTX, and MTX. This analysis was conducted indirectly by quantifying the fluorescence of the carboxy H_2-DCFDA reagent, which is reduced by the ROS generated in the cell cytoplasm and results in DCF,

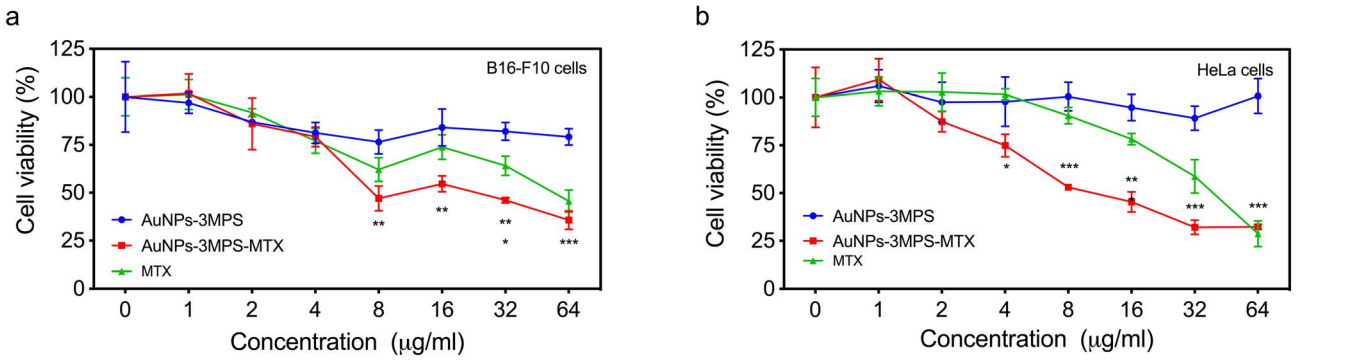

Fig. 1 Cell viability of (a) melanoma B16-F10 and (b) cervix HeLa cells exposed to different concentrations of AuNPs, AuNPs-MTX, and MTX. Results are expressed as the mean ± SD ($n = 3$), **$p < 0.01$; ***$p < 0.001$ using two-way ANOVA with Tukey's comparison test.

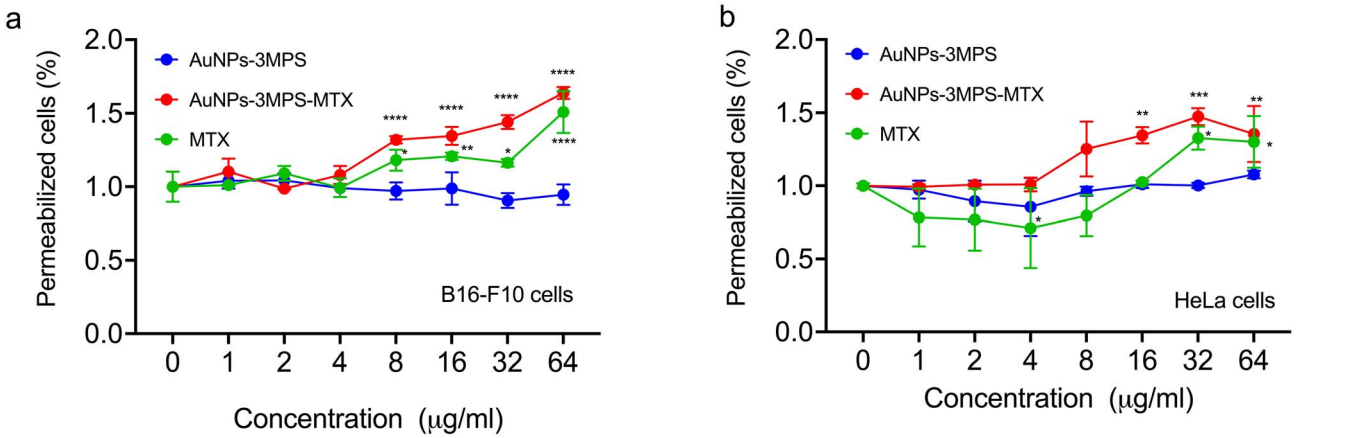

Fig. 2 Cell permeability of (a) melanoma B16-F10 and (b) cervix HeLa cells exposed to different concentrations of AuNPs, AuNPs-MTX, and MTX. Results are expressed as the mean ± SD ($n = 3$), **$p < 0.01$; ***$p < 0.001$ using two-way ANOVA with Tukey's comparison test.

a fluorogenic compound. The results demonstrate the capability of AuNPs to induce significant oxidative stress. As shown in Fig. 3a, the B16-F10 melanoma cell line incubated with AuNPs-3MPS-MTX exhibited an increase in ROS production compared to AuNPs-MPS counterpart. ROS production significantly increased at concentrations ranging from 8, to 64 μg

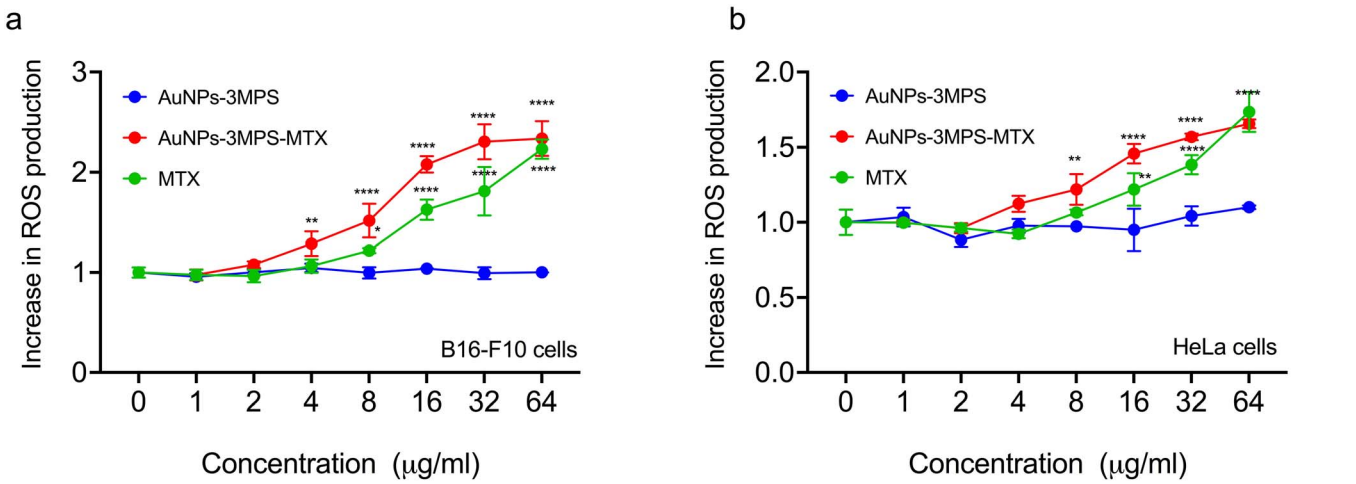

Fig. 3 ROS production of (a) melanoma B16-F10 and (b) cervix HeLa cells exposed to different concentrations of AuNPs, AuNPs-MTX, and MTX. Results are expressed as the mean ± SD ($n = 3$), **$p < 0.01$; ***$p < 0.001$ using two-way ANOVA with Tukey's comparison test.

mL^{-1} of AuNPs-3MPS-MTX. In contrast, the percentage of ROS produced by HeLa cell line exposed to the same concentrations of AuNPs-3MPS-MTX displayed an increase in ROS production within the concentration range of 2 to 64 μg mL^{-1} AuNPs-MPS.

Determination of cell death by apoptosis and necrosis for B16F10 and HeLa cells

Cell death was assessed for both cell lines, using AuNPs-3MPS, MTX and the proposed system AuNPs-3MPS-MTX. Fig. 4a shows

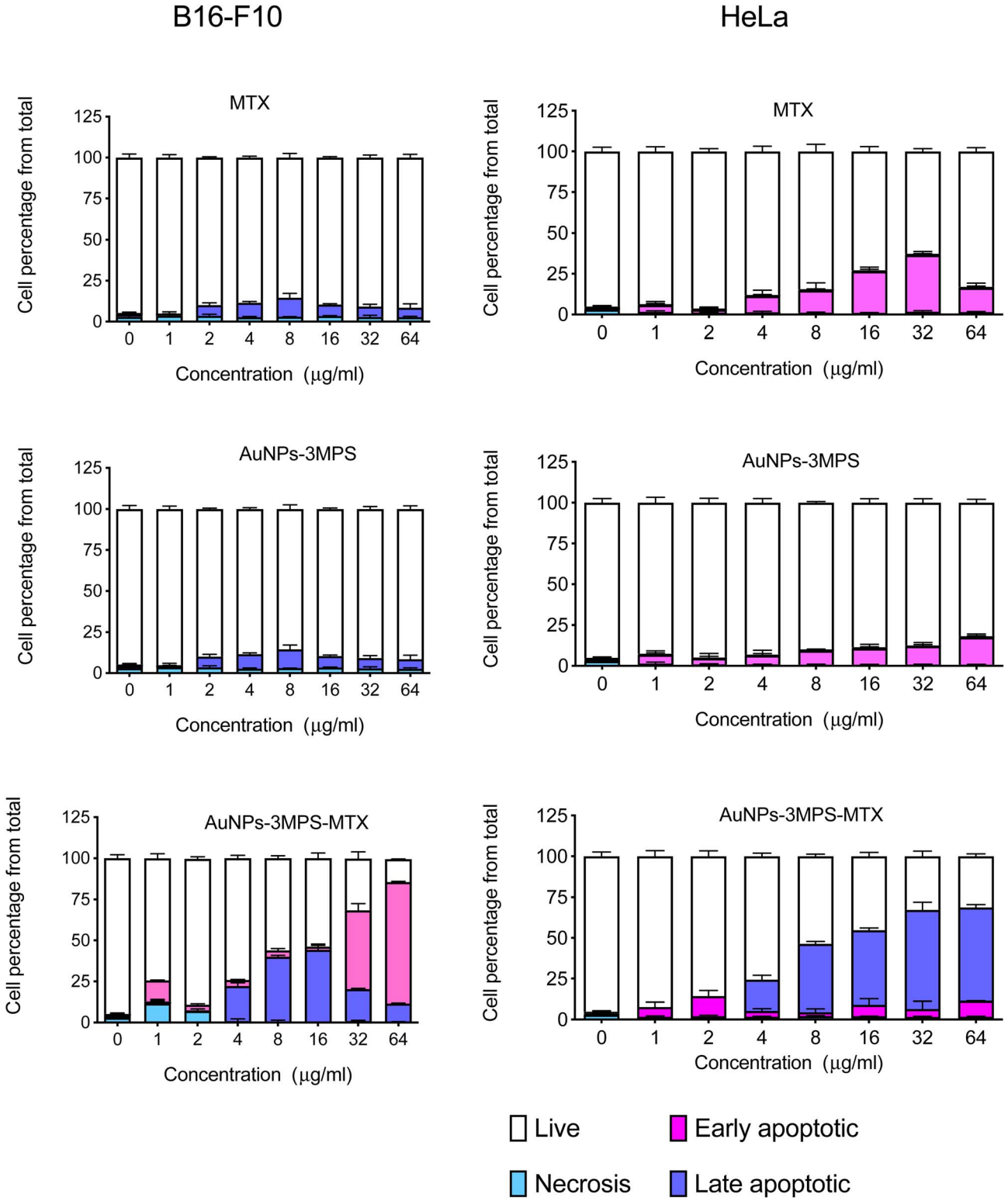

Fig. 4 Cell death of (a) melanoma B16-F10 and (b) cervix HeLa cells exposed to different concentrations of AuNPs, AuNPs-MTX, and MTX. Results are expressed as the mean ± SD ($n = 3$).

the results for the B16-F10 melanoma cell line, indicating no significant differences in cell death values when different concentrations of AuNPs-3MPs and MTX were used. The cell death remained below 10%. However, when B16-F10 cells were treated with various concentrations of AuNPs-3MPS-MTX ranging from 4 to 64 μg mL^{-1}, it triggered apoptosis in more than 50% of the cells.

In Fig. 4b, the effect of AuNPs-3MPS and MTX on HeLa cells was observed. In this case, HeLa cells were more susceptible to MTX compared to B16-F10 cells. MTX at higher concentrations from 16 to 64 μg mL^{-1} induced early apoptosis in more than 25% of the cells. However, when HeLa cells were exposed to different concentrations of AuNPs-3MPS-MTX, late apoptosis was the primary mode of cell death. The results indicate that HeLa cells are more susceptible to the effects of the proposed nanosystem AuNPs-3MPS-MTX than melanoma B16-F10 cells.

Determination of internalization of AuNPs into B16F10 and HeLa cells

We conducted flow cytometry analysis to determine the capability of AuNPs-3MPS-MTX to be taken up by cancer cells. The uptake of nanoparticles by cells has been previously investigated using flow cytometry, a technique that allows us to compare the intracellular complexity, often referred to as granularity, among different cell populations[22,23] Flow cytometry measurements, specifically the side scattering (SSC), are directly linked to intracellular complexity. Consequently, we could compare the vesicle content of control cells with the intracellular complexity of cells exposed to AuNPs-3MPS-MTX. Fig. 5 compares the percentage of cells that have internalized AuNPs-3MPS-MTX, AuNPs-3MPS, and free MTX. As depicted, AuNPs-3MPS-MTX were internalized by melanoma B16-F10 and HeLa cancer cells. In contrast, no evidence suggests that MTX changes the cytoplasmic content of both cell lines.

Biocompatibility

The bioinert characteristic of gold offers nanoparticle formulations that are essentially non-toxic and non-immunogenic making gold nanoparticles suitable for exploratory *in vitro* and *in vivo* studies.[24,25] In this context, the effect on cell viability was studied for B16-F10 melanoma and HeLa cells. Since one of the most common applications of AuNPs is in the vectorization and targeting of drugs, this study used methotrexate (MTX) as the active substance for cancer treatment. The MTT test, a colorimetric technique measuring the reduction of MTT to determine mitochondrial activity, was used for this assay. Compared to free-MTX, AuNPs are biocompatible as established previously in the literature.[16] However, when the effect of the nanosystem AuNPs-3MPS-MTX was evaluated for B16-F10 melanoma cell lines, a diminishment in cell viability was observed in a concentration-dependent manner, with lower cell viability presented at higher concentrations of the nanosystem. This indicated that AuNPs-3MPS-MTX was toxic to B16-F10 melanoma cell line which is considered one of the most aggressive cancers[26] as described by Miooc, M., *et al.* (2018). In that study, the authors reported that concentrations higher than 100 μg mL^{-1} of surface-modified betulin-conjugated gold nanoparticles, induced a notably decrease in cell viability. In contrast, when the nanosystem AuNPs-3MPS-MTX was used, a significant reduction of cell viability was observed at 8 μg mL^{-1}, which was even higher than the effect caused by free MTX.

On the other hand, when compared to free MTX, HeLa cells exhibited a higher susceptibility to the nanosystem AuNPs-3MPS-MTX at 4 μg mL^{-1}. This decrease in cell viability indicates that the drug is being targeted to the HeLa cells and also exerting its effects on them. This effect could be associated with the shape of the AuNPs, as demonstrated by Zhao, X. F, *et al.* (2019). In their study, the authors observed a decrease in cell viability in HeLa cells when MTX was used in conjunction with AuNPs, as opposed to using MTX alone.[27] A correlation between the morphology and functionalization of AuNPs with their cytotoxic effect was described[28] by Siddique, S., *et al.* (2020). In that review, the authors stated that the size, shape, and functionalization of the NPs modify their effectiveness.[28,29] In this work, spherical 5 nm AuNPs-3MPS were loaded with MTX

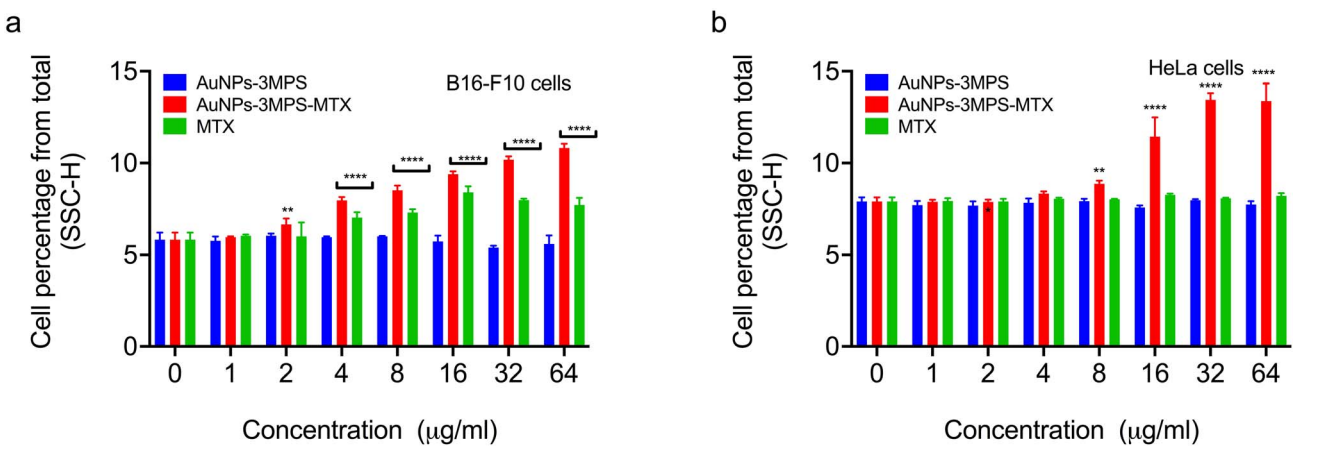

Fig. 5 Internalization of nanoparticles into (a) melanoma B16-F10 and (b) cervix HeLa cells exposed to different concentrations of AuNPs, AuNPs-MTX, and MTX. Results are expressed as the mean ± SD ($n = 3$). $^{**}p < 0.01$; $^{***}p < 0.001$ using two-way ANOVA with Tukey's comparison test.

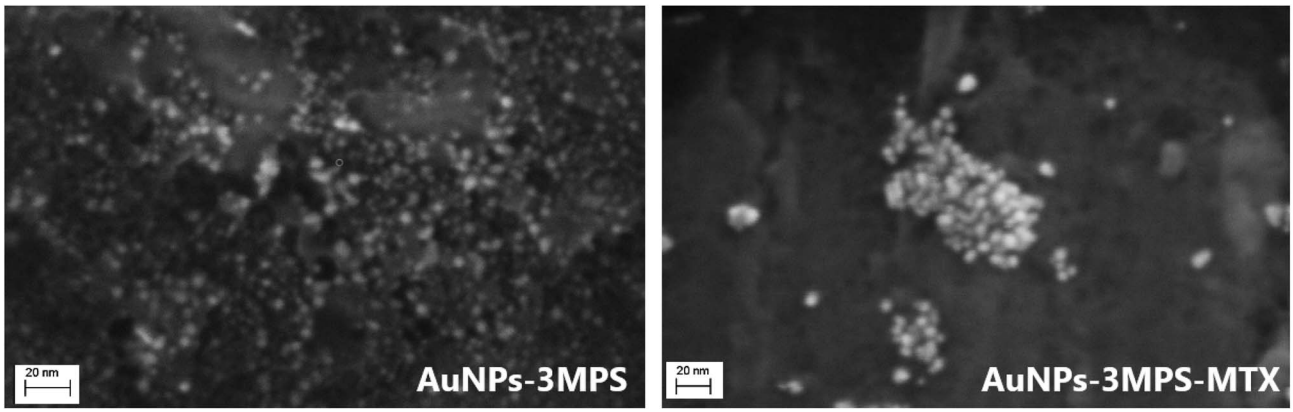

Fig. 6 FE-SEM images of pristine and MTX loaded AuNPs-3MPS.

lipophilic drug thereby increasing its bioavailability (Fig. 6: SEM images of pristine and MTX loaded AuNPs-3MPS). The choice of direct functionalization with highly hydrophilic thiols significantly reduces the possible cytotoxicity of the gold nanoparticles.[16]

In addition, the 3MPS functionalizing agent act as a platform for post-synthesis conjugation of MTX *via* electrostatic binding (between protonated aromatic $-NH_2$ groups in the ring structure of MTX and negatively charged $-SO_3^-$ moieties), leading to the formation of large clusters with densely packed arrangement of AuNPs-3MPS-MTX, in agreement with literature results.[19]

The size of the system was an important factor for its permeability in the studied cells, leading to an adequate release of the active substance used for programmed cell death and countering the proliferation of malignant cells at lower concentrations of MTX in HeLa cells.

Furthermore, this study investigated membrane permeability due to the crucial role of nanomaterial-cell and lipid bilayer interactions in various applications, such as phototherapy, imaging, and drug/gene delivery. These applications require precise control over nanoparticle–cell interactions, which primarily depend on the surface properties of nanoparticles.[30] Moreover, the decrease in cell viability could be attributed to oxidative stress induced by reactive oxygen species, as reported previously in the literature.[31,32] It has been suggested that the ability of NPs to induce toxicity is linked to their higher surface reactivity, where smaller particles with larger surface areas per unit mass produce more reactive oxygen species in the cellular environment, leading to greater cell death. As mentioned earlier, the proposed nanosystem has a hydrodynamic diameter of approximately 5 nm, contributing to reducing malignant cell proliferation. The interactions of the nanomaterial with cell membranes are determined not only by its shape and size but also by the chemical functionalities of its surface. The proposed nanosystem demonstrated a slight increase in the percentage of permeabilized cells, indicating its effectiveness in penetrating the cell membrane in both cell lines. This beneficial effect on cell permeability can be attributed to the size and shape of the nanomaterial during its interaction with cells as confirmed by Kimura, N. *et al.*, 2018, in their study.[33] They used liposomes with a diameter of 25 nm for delivering the active substance in tumor treatment, resulting in a lower penetration percentage.

On the other hand, Jain, A. K. *et al.*, 2019 investigated the effectiveness of drug carrier vehicles such as silica nanoparticles and calcium phosphate nanoparticles (CaP) obtaining NPs sizes ranging from 8 to 20 nm.[34] They achieved an effective percentage of permeabilized cells at smaller size. The authors concluded that the size and shape of the NPs were critical in enhancing the effectiveness of the delivered active substance.

After determining the decrease in cell viability, the increase in reactive oxygen species, and the effective penetration of the proposed nanosystem into the cell membrane. Identifying the type of cell death caused by the proposed nanosystem becomes essential. Cell death is a fundamental part of the cell life cycle, crucial for maintaining homeostasis. Necrosis represents an accidental or non-programmed type of cell death, occurring when external factors surpass the physiological conditions of the tissue, subjecting the cell to excessive and uncontrollable stress. On the other hand, apoptosis is the most extensively studied form of programmed cell death, as it maintains the physiological balance between cell proliferation and elimination.

Various substances, including death-inducing ligands, nucleic acids, ROS, inflammatory mediators, toxins, and drugs, among other substances, activate mechanisms leading the cell to its destruction. Based on the results obtained in this study late apoptosis was observed at concentrations ranging from 4 to 64 $\mu g\ mL^{-1}$ for HeLa cells, indicating higher susceptibility compared to B16-F10 melanoma cells. The presence of late apoptosis at higher concentrations suggests that the AuNPs-3MPS-MTX nanosystem is effective in reducing live cells and effectively programming cell death. This characteristic prevents an imbalance in the cellular environment. Therefore, the use of the proposed nanosystem shows promise in promoting programmed cell death effectively.

In this regard, Liu C. M., *et al.* 2019, developed a single core/shell-structured nanoparticle for prostate cancer treatment.[35] Their approach involved using a mesoporous silica nanoparticle

core as a container to encapsulate drugs, including doxorubicin (DOX), along with highly efficient $CaCO_3$. Their study demonstrated remarkable antitumor efficacy through live/dead cell detection, and their apoptosis experiment revealed that the proposed material effectively induced apoptosis-related death in prostate cancer cells.

Apoptosis is a process wherein the DNA of cells in the nucleus is cleaved into smaller fragments, and certain cell organelles, such as the endoplasmic reticulum, break down into fragments as well. Eventually, the entire cell divides into small pieces, each meticulously wrapped in a membrane bundle. The present work indicates that the proposed nanosytem AuNPs-3MPS-MTX likely achieves a similar arrangement, mitigating the risk of cellular imbalance.

4. Conclusions

Highly hydrophilic, small, stable, and non-cytotoxic AuNPs-3MPS as drug carriers hold promising potential for treating cervical cancer and melanoma. While free AuNPs-3MPS showed no cytotoxicity whereas the AuNPs-3MPS-MTX nanoconjugate exhibited a more potent effect than free MTX. The active role of AuNPs-3MPS in drug delivery was evidenced by permeation studies, which demonstrated improved drug penetration inside cells. As previously reported,[16] the functionalized AuNPs-3MPS had an average hydrodynamic size of 5 nm. These nanosystem characteristics and properties induced cytotoxicity, likely attributed to the increased reactive oxygen species for both cell lines studied. Moreover, the size of the nanosystem played a crucial role in its permeability into the cells, leading to programmed cell death and countering the proliferation of malignant cells. In HeLa cells the proposed nanosystem demonstrated a more significant decrease in cell viability by late apoptosis than the B16F10 cell line. This observation suggests that the proposed system effectively targets and releases MTX, enhancing the therapeutic effect for both B16-F10 and HeLa cells. This supports its potential as a valuable approach for targeted drug delivery and cancer treatment.

Credit author statement

M. J. Hernández-Esparza: formal analysis and research, writing. Ilaria Fratoddi: conceptualization, methodology, writing—review and editing. Sara Cerra: investigation. K. Juarez-Moreno: research, data curation, writing—review and editing. R. Huirache-Acuña: conceptualization, funding acquisition, writing—review and editing.

Conflicts of interest

The authors declare no competing interest regarding the publication of this paper.

Acknowledgements

Dr R. Huirache-Acuña wants to thank to CIC-UMSNH 2023 and PICIR-047 Projects for their financial support. The financial support of this work was provided by the following projects: CIC-UMSNH 2023 and PICIR-047 Projects. IF and SC acknowledge the financial support of Sapienza University of funding Grant Ateneo Ricerca 2020 (RM120172B6B660AB) and Ateneo Ricerca 2022 (RM1221867C322C1). Dr K. Juarez-Moreno acknowledges the financial support provided by PAPIIT-UNAM AI204223.

References

1 J. J. Liang, Y. Y. Zhou, J. Wu and Y. Ding, *Drug Metab. Curr.*, 2014, **15**, 620–631.
2 N. Bawarski, E. Chidlowsky, D. J. Bharali and S. A. Mousa, Emerging nanopharmaceuticals, *Nanomedicined*, 2008, **4**, 273–282.
3 P. M. Ajayan, J. M. Lambert, P. Bernier, L. Barbedette, C. Colliex and J. M. Planeix, *Chem. Phys. Lett.*, 1993, **215**, 509–517.
4 M. Moddaresi, M. B. Brown, Y. Zhao, S. Tamburic and S. A. Jones, *Int. J. Pharm.*, 2010, **400**(1–2), 176–182.
5 S. D. Brown, P. Nativo, J.-A. Smith, D. Stirling, P. R. Edwards, B. Venugopal, D. J. Flint, J. A. Plumb, D. Graham and N. J. Wheate, *J. Am. Chem. Soc.*, 2010, **132**(13), 4678–4684.
6 V. Ramalingam, K. Varunkumar, V. Ravikumar and R. Rajaram, *Sci. Rep.*, 2018, **8**, 3815.
7 S. Kumar Vemuria, R. Reddy Banala, S. Mukherjee, P. Uppula, G. P. V. Subbaiah, A. V. Gurava Reddy and T. Malarvilli, *Mater. Sci. Eng., C*, 2019, **99**, 417–4298.
8 L. Ye and Q. Song, *Int. J. Clin. Exp. Med.*, 2015, **8**(7), 10501–10507.
9 I. Maria, M. Paino, V. S. Marangoni, R. d. Cássia, S. de Oliveira, L. Maria, G. Antunes and V. Zucolotto, *Toxicol. Lett.*, 2012, **215**(2), 119–125.
10 X. Zhao, J. Pan, W. Li, W. Yang, L. Qin and Y. Pan, *Int. J. Nanomedicine*, 2018, **13**, 6207–6221.
11 F. Naz, A. K. Dinda, A. Kumar and V. Koul, *Int. J. Pharm.*, 2019, **569**, 118561.
12 Yu, J. Yu, Y. Yi, T. Chen, L. Yu, W. Zeng, X. Ouyang, C. Huang, S. Sun, Y. Wang, Y. Liu, C. Lin, M. Wu and M. Lin, *J. Control. Release.*, 2022, **347**, 104–114.
13 Chen, W. Zeng, C. Tie, M. Yu, H. Hao, Y. Deng, Q. Li, H. Zheng, M. Wu and M. Lin, *Bioact. Mater.*, 2022, **10**, 515–525.
14 X. Zeng, M. Luo, G. Liu, X. Wang, W. Tao, Y. Lin, X. Ji, L. Nie and L. Mei, *Adv. Sci.*, 2018, **5**, 1800510.
15 Q. Li, Z. Shi, F. Zhang, W. Zeng, D. Zhu and M. Lin, *Acta Pharm. Sin. B*, 2022, **12**(1), 107–134.
16 T. A. Salamone, L. Rutigliano, B. Pennacchi, S. Cerra, R. Matassa, S. Nottola, F. Sciubba, C. Battocchio, M. Marsotto, A. Del Giudice, A. Chumakov, A. Davydok, S. Grigorian, G. Canettieri, E. Agostinelli and I. Fratoddi, *J. Colloid Interface Sci.*, 2023, **649**, 264–278.
17 H. Bessar, I. Venditti, L. Benassi, C. Vaschier, P. Azzoni, G. Pellacani, C. Magnon, E. Botti, V. Casagrande, M. Federici, A. Costanzo, L. Fontana, G. Testa, F. M. Fawzia, I. S. Ali, R. M. Vittoria and I. Fratoddi, *Colloids Surf., B*, 2016, **141**, 141–147.

18 M. Magogotya, M. Vetten, M. P. Roux-van der Merwe, J. Badenhorst and M. Gulumian, *Mutation Research/Genetic Toxicology and Environmental Mutagenesis*, 2022, **883–884**, 503556.
19 S. Cerra, R. Matassa, A. M. Beltrán, G. Familiari, C. Battocchio, I. Pis, F. Sciubba, F. A. Scaramuzzo, A. Del Giudice and I. Fratoddi, *Mater. Sci. Eng. C-Mater. Biol. Appl.*, 2020, **117**, 111337.
20 I. Fratoddi, L. Benassi, E. Botti, C. Vaschieri, I. Venditti, H. Bessar, M. A. Samir, P. Azzoni, C. Magnoni, A. Constanzo, V. Casagrande, M. Federici, L. Bianchi and G. Pellacani, *Nanomed. Nanotechnol. Biol. Med.*, 2019, **17**, 276–286.
21 D. Chávez-García, K. J. Moreno, I. C. Osuna, P. Navarro and G. A. Hirata, *J. Biomed. Mater. Res., Part B*, 2020, **108**(6), 2396–2406.
22 A. Kumar, A. K. Pandey, S. S. Singh, R. Shanker and A. Dhawan, *Chemosphere*, 2011, **83**(8), 1124–1132.
23 H. Suzuki, T. Toyooka and Y. Ibuki, *Environ. Sci. Technol.*, 2007, **41**(8), 3018–3024.
24 A. M. Alkilany and C. J. Murphy, *J. Nanopart. Res.*, 2010, **12**(7), 2313–2333.
25 B. Lee, G. Yoon, S. W. Lee, S. Y. Jeong, B. C. Ahn, D. K. Lim, J. Lee and Y. H. Jeon, *Small*, 2016, **12**(35), 4894–4901.
26 M. Mioc, I. Z. Pavel, R. Ghiulai, D. E. Coricovac, C. Farcaș, C. V. Mihali, C. Oprean, V. Serafim, R. A. Popovici, C. A. Dehelean, M. I. Shtilman, A. M. Tsatsakis and C. Șoica, *Front. Pharmacol*, 2018, **9**, 429.
27 X. F. Zhao, Z. L. Liu, X. D. Li, S. P. Li and F. G. Song, *J. Phys. Chem. Solids*, 2019, **124**, 73–80.
28 S. Siddique and J. C. Chow, *Appl. Sci.*, 2020, **10**(11), 3824.
29 D. Mandal, A. Maran, M. J. Yaszemski, M. E. Bolander and G. Sarkar, *J. Mater. Sci.: Mater. Electron.*, 2008, **20**, 347–350.
30 K. Juárez-Moreno, D. Chávez-García, G. Hirata and R. Vázquez-Duhalt, *Toxicol. in Vitro*, 2022, **85**, 105461.
31 M. N. O'Brien, M. R. Jones, K. A. Brown and C. A. Mirkin, *J. Am. Chem. Soc.*, 2014, **136**(21), 7603–7606.
32 N. Pandiyan, B. Murugesan, M. Arumugam, J. Sonamuthu, S. Samayanan and S. Mahalingam, *J. Mol. Liq.*, 2020, **312**, 113245.
33 N. Kimura, M. Maeki, Y. Sato, Y. Note, A. Ishida, H. Tani, H. Harashima and M. Tokeshi, *ACS Omega*, 2018, **3**(5), 5044–5051.
34 R. K. Jain and S. Thareja, *Artif. Cells, Nanomed., Biotechnol.*, 2019, **47**(1), 524–539.
35 C. M. Liu, G. B. Chen, H. H. Chen, J. B. Zhang, H. Z. Li, M. X. Sheng, W. B. Weng and S. M. Guo, *Colloids Surf., B*, 2019, **175**, 477–486.